# Effect of Polarization Dependent Loss on the Quality of Transmitted Polarization Entanglement

Brian T. Kirby ⓘ, Daniel E. Jones, *Member, OSA*, and Michael Brodsky, *Fellow, OSA*

*(Post-Deadline Paper)*

*Abstract*—**Quantum networking brings together several diverse research areas, such as fiber-optic communication, quantum optics, and quantum information, to achieve capabilities in security, secret sharing, and authentication which are unavailable classically. The development of practical fiber-based quantum networks requires an understanding of the reach, rates, and quality of the entanglement of distributed quantum states. Here, we present a theoretical model describing how the magnitude and orientation of polarization dependent loss (PDL), a common impairment in fiber-optic networks, affects the entanglement quality of distributed quantum states. Furthermore, we theoretically characterize how PDL in one fiber channel can be optimally applied in order to nonlocally compensate for the PDL present in another channel. We present experimental results that verify our theoretical model.**

*Index Terms*—**Optical fiber communication, quantum entanglement.**

## I. INTRODUCTION

**Q**UANTUM networks promise to offer functionalities unavailable classically by using distributed quantum entanglement as a resource [1]. Essential to the development of a quantum network is the ability to create, manipulate, and distribute entanglement between distant nodes [2]. It would be desirable to leverage the vast deployed fiber optics infrastructure for entanglement distribution. However, entanglement is fragile, and a greater understanding of how transmission through fibers and fiber components affects entanglement quality is required in order to successfully develop a fiber-based quantum network. Specifically, for the distribution of polarization-entangled states, polarization mode dispersion (PMD) and polarization dependent loss (PDL) are the two principal effects which must be accounted for [3]–[5].

While the PDL of the fibers itself is often low, PDL is commonly found in optical components, such as isolators, multiplexers, and couplers, where the attenuations of the two orthogonal polarization modes can differ. The effects of PDL in classical communication have been thoroughly investigated over the

years [6]–[12]. However, PDL has only received limited attention in the domain of quantum communication and has mainly been studied via the method of the antinormally-ordered quantum characteristic function [13]. This is partially due to the cumbersome nature of calculations involving two-photon states, since the relative orientation of PDL elements in the fiber channel of each photon needs to be considered. We note, however, that for polarization entanglement, a single PDL element is itself an example of a more general operation known as local filtering [14]–[20], in which an element called a filter preferentially selects one mode of a superposition quantum state over the other.

Local filtering operations on entangled states have largely been of interest due to their ability to probabilistically increase the entanglement of a quantum state [14]–[17]. Entanglement distillation of this type, for some pure and mixed states, has been demonstrated experimentally [21]. In these studies, the filtering elements are controlled, and the aim is to probabilistically increase the entanglement of a given state. This is in contrast to the situation in optical networks where the filtering elements, in the form of PDL elements, are both randomly oriented and subject to change with time, and cannot be fully controlled.

Here, we present a compact description of how PDL of any orientation affects the entanglement of both pure and mixed states of polarization-entangled photons in the Bell-diagonal form. The Bell-diagonal states are of particular importance because they encompass the ideal Bell states as well as states resulting from an ideal state which experiences various common impairments such as depolarizing noise, decoherence, and application of PMD [22]–[23]. More specifically, we consider a system comprised of an initial two-photon polarization-entangled state where each photon is transmitted through a different channel which may contain PDL of arbitrary orientation and magnitude. In the following, we analyze the relationship between entanglement, PDL orientation, and PDL magnitude for several classes of ideal and impaired states. Then we experimentally verify our theory using a fiber-based source of polarization-entangled photons both with and without PMD present. We further determine the optimal system configuration that allows PDL acting in one channel of the system to fully or partially compensate for the entanglement lost due to PDL present in the other channel. We term this unique feature of quantum systems nonlocal PDL compensation.

This paper is organized as follows. In Section II, we introduce the general theory of PDL and obtain a simple expression for

the entanglement of a two-photon polarization-entangled state undergoing PDL of arbitrary orientation and magnitude. In this section, we emphasize that all possible orientations of two PDL elements, one in the channel for each photon of an entangled state, can be parameterized into a single variable. In Section III, we find the conditions which allow for the maximum recovery of the entanglement lost due to PDL acting on one photon of an entangled pair through the addition of another PDL element acting on the other photon. In Section IV, we present an experimental demonstration of these results using a fiber-based source of polarization-entangled qubits. Finally, we conclude in Section V.

## II. GENERAL THEORY

### A. Entanglement Expressions

Polarization dependent loss (PDL) occurs when the transmission coefficient of a medium or a waveguide depends on the polarization of the input light. This effect is quantified in decibels as $p = 10 \log_{10} (I_{\max}/I_{\min})$ where $I_{\max}$ and $I_{\min}$ are the maximum and minimum transmitted intensities of light with respect to all possible input polarizations. In general, the polarization state with maximum transmission can point in any direction $\hat{\gamma}$ in Stokes space, and has the corresponding PDL operator [3]:

$$\boldsymbol{P} = e^{-\gamma/2} e^{\frac{1}{2}\vec{\gamma}\cdot\vec{\boldsymbol{\sigma}}} = e^{-\gamma/2}(\boldsymbol{I}_2 \cosh(\gamma/2) + (\hat{\gamma}\cdot\vec{\boldsymbol{\sigma}})\sinh(\gamma/2))$$

(1)

where $\vec{\boldsymbol{\sigma}}$ is a vector of the Pauli matrices, $\boldsymbol{I}_2$ is the two dimensional identity matrix, $\vec{\gamma} = \gamma\hat{\gamma}$, $p = \gamma(20\log_{10}e)$, and we assume $\gamma \geq 0$.

We are interested in assessing how the entanglement of a two-photon polarization-entangled state is impacted by the presence of PDL in the transmission channel of each photon. Ideally, states distributed for quantum information processing tasks would be both pure and perfectly entangled. The canonical examples of such states are the Bell states, defined in the $\{H, V\}$ basis as $|\Psi^{\pm}\rangle = (|HV\rangle \pm |VH\rangle)/\sqrt{2}$ and $|\Phi^{\pm}\rangle = (|HH\rangle \pm |VV\rangle)/\sqrt{2}$. With these definitions, we can intuitively understand how PDL decreases the entanglement of a quantum state. To begin, consider that if we were to measure the first photon of a $|\Phi^+\rangle$ state in the $\{H, V\}$ basis, we would find either outcome ($H$ or $V$) with equal probability. However, if we were to first pass this qubit through a PDL element oriented such that it preferentially absorbs $H$ polarized photons, then clearly we would no longer detect either outcome with equal probability. More specifically, after post selection, meaning in the case when instances where a photon is absorbed by the PDL element are ignored, the final state would become $|\Phi'^+\rangle = \alpha|HH\rangle + \beta|VV\rangle$ with $|\alpha| < |\beta|$, which is no longer a Bell state.

Realistically, however, decoherence mechanisms in the transmission channel can cause these states to mix. In this case, the states are most easily described using a density matrix of the form $\boldsymbol{\rho} = \sum_i p_i |\psi_i\rangle\langle\psi_i|$, where $p_i$ is a classical probability and $|\psi_i\rangle$ represents a pure quantum state. Specifically, it has been shown that Bell states undergoing polarization mode dispersion (PMD) become a particular type of mixed state known as a

Bell-diagonal state [22]–[23]. Hence, our analysis is focused on these states.

Bell-diagonal states are those that can be written as a mixture of the Bell states. Specifically, this means that any Bell-diagonal state can be expressed as a convex sum of the form $\boldsymbol{\rho}_{BD} = a_1|\Phi^+\rangle\langle\Phi^+| + a_2|\Phi^-\rangle\langle\Phi^-| + a_3|\Psi^+\rangle\langle\Psi^+| + a_4|\Psi^-\rangle\langle\Psi^-|$. We find that expanding these states in terms of the Pauli matrices will be useful for what follows. To this end, the Bell-diagonal states can alternatively be expressed as [25]:

$$\boldsymbol{\rho}_{BD} = \frac{1}{4}\left(\boldsymbol{I}_2 \otimes \boldsymbol{I}_2 + \sum_{i=1}^{3} t_i\boldsymbol{\sigma}_i \otimes \boldsymbol{\sigma}_i\right),$$

(2)

where the $\boldsymbol{\sigma}_i$ define the Pauli matrices and $\otimes$ indicates the tensor product of the two Hilbert spaces, each associated with one photon of the pair. The diagonal matrix $\boldsymbol{T} = \text{diag}(t_1, t_2, t_3)$ is referred to as the correlation matrix and plays an important role in determining how PDL orientation affects the entanglement of a state.

The entanglement between two quantum states can be quantified in terms of the entanglement of formation, which is physically related to the number of maximally entangled states needed as a resource to create a copy of a given state. For the special case of two qubits, it has been shown that the entanglement of formation is a monotonic function of another entanglement measure, which is often simpler to calculate but lacks a physical interpretation, known as the concurrence [26]. The concurrence is defined as $C(\boldsymbol{\rho}) = \max(0, \sqrt{\lambda_1} - \sqrt{\lambda_2} - \sqrt{\lambda_3} - \sqrt{\lambda_4})$, where the $\lambda_i$ are the eigenvalues of $\boldsymbol{\rho}(\boldsymbol{\sigma}_y \otimes \boldsymbol{\sigma}_y)\boldsymbol{\rho}^*(\boldsymbol{\sigma}_y \otimes \boldsymbol{\sigma}_y)$, with $\lambda_1 \geq \lambda_2 \geq \lambda_3 \geq \lambda_4$ and $\boldsymbol{\sigma}_y$ given by the usual Pauli matrix. A concurrence of 0 indicates that the state is separable, meaning it has no entanglement, and a concurrence of 1 indicates that the state is maximally entangled. The calculation of this quantity for a two-qubit state undergoing arbitrary local filtration on each qubit was performed in [18]. Adapting that result to the notation of Eq. (1) and restricting ourselves to the Bell-diagonal states of Eq. (2), we obtain the concurrence as:

$$C(\boldsymbol{\rho}) = \frac{C(\boldsymbol{\rho}_0)}{\cosh(\gamma_A)\cosh(\gamma_B) + \sinh(\gamma_A)\sinh(\gamma_B)\kappa},$$

(3)

where the $\vec{\gamma}_{A,B}$ define the PDL in the two channels and $\boldsymbol{\rho}_0$ is the state before PDL is applied: $\boldsymbol{\rho} \propto (\boldsymbol{P}_A \otimes \boldsymbol{P}_B)\boldsymbol{\rho}_0(\boldsymbol{P}_A \otimes \boldsymbol{P}_B)^{\dagger}$. We define $\kappa = \sum_{i=1}^{3} \gamma_{Ai}\gamma_{Bi}t_i$, where $\gamma_{Ai}$ ($\gamma_{Bi}$) are the components of $\hat{\gamma}_A$ ($\hat{\gamma}_B$) along the Cartesian basis in Stokes space. All dependence of Eq. 3 on PDL orientation is encapsulated in $\kappa$ alone. Much of the remainder of this paper is focused on understanding how $\kappa$ changes with the relative orientation of PDL elements, and how this affects the concurrence of the overall state.

It is interesting to note that when PDL is present in only one of the two quantum channels, the concurrence expression in Eq. (3) simplifies to an orientation-independent form. Indeed, setting one of the two PDL elements, in this case $\gamma_B$, to zero in Eq. (3) results in:

$$C(\boldsymbol{\rho}) = \frac{C(\boldsymbol{\rho}_0)}{\cosh(\gamma_A)}.$$

(4)

Therefore, the entanglement in a system consisting of a Bell-diagonal state and a single PDL element cannot be changed through rotation of that PDL element alone. Intuitively, this rotational invariance can be understood as a result of the depolarized nature of the individual photons in a Bell-diagonal state.

We study the dependence of the concurrence on PDL elements (Eq. (3)) for three following special cases of the Bell-diagonal states that are of physical importance. Those are Bell states, Werner states, and rank-2 Bell-diagonal states. Werner states result from the often physically-realized case of adding completely depolarized noise to both photons of a Bell state. Rank-2 Bell-diagonal states commonly arise from bit-flipping errors, general coherence or, in some cases, from application of PMD [23]. Now, we consider the corresponding elements $t_i$ of the correlation matrix $T$ when each of these classes of states is written in the form of Eq. (2). The Bell states, which were introduced above as $|\Psi^\pm\rangle$ and $|\Phi^\pm\rangle$, satisfy $|t_i| = 1$ for all $i$ when written in the form of Eq. (2). Werner states are conventionally expressed as:

$$\boldsymbol{\rho}_W = \nu|\chi\rangle\langle\chi| + \frac{1-\nu}{4}I_4, \qquad (5)$$

where $|\chi\rangle$ is any one of the Bell states. In the form of Eq. (2), they produce $|t_i| = \nu$ for all $i$. Traditionally, Werner states are defined with $\chi = \Psi^-$; here, however, we refer to the states defined in Eq. (5) as Werner states since they are equivalent to traditional Werner states up to local rotations and therefore behave similarly in the following analysis. Finally, the rank-2 Bell-diagonal states, also known as edge states [27], are expressed as:

$$\boldsymbol{\rho}_{R2} = \frac{1+C_{R2}}{2}|\chi_1\rangle\langle\chi_1| + \frac{1-C_{R2}}{2}|\chi_2\rangle\langle\chi_2|, \qquad (6)$$

where $\chi_1$ and $\chi_2$ are again any of the four Bell states, as long as $\chi_1 \neq \chi_2$, and $C_{R2}$ is the concurrence of the rank-2 state. These states have a single component $|t_i| = 1$, and the other two $|t_{j \neq i}| = C_{R2}$.

## B. Dependence of Entanglement on Polarization Dependent Loss Orientation

The dependence of concurrence on PDL orientation can be understood through an examination of $\kappa$ alone, since all orientation dependence of Eq. (3) is contained within $\kappa$. Therefore, the range of values that $\kappa$ can take for a given system determines the range of concurrences that are accessible through local rotations on that system, given an initial Bell-diagonal state and a separate channel for each qubit with arbitrary PDL. In an effort to characterize $\kappa$ and the range of values it can take, we rewrite $\kappa$ in a vectorial form, allowing the coherence matrix to be interpreted as an operator acting on the unit Stokes vectors of the PDL elements:

$$\kappa = \sum_{j=1}^{3} \gamma_{Aj}\gamma_{Bj}t_j = (\boldsymbol{T}\hat{\gamma}_A) \cdot \hat{\gamma}_B = ||\boldsymbol{T}\hat{\gamma}_A||\cos(\theta), \qquad (7)$$

where $||\cdot||$ indicates the vector magnitude and $\theta$ defines the angle between $\boldsymbol{T}\hat{\gamma}_A$ and $\hat{\gamma}_B$. We note that our choice to group $\boldsymbol{T}$ and $\hat{\gamma}_A$ in Eq. (7) is arbitrary, and we could instead chose $\hat{\gamma}_B$
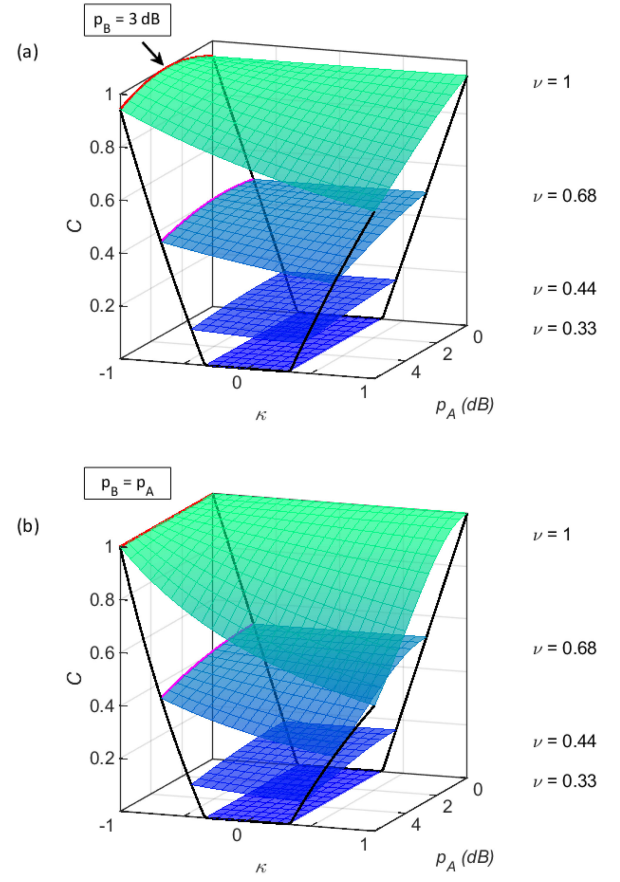


Fig. 1. Concurrence as a function of PDL orientation ($\kappa$) and PDL magnitude in channel A ($p_A$). Colored surfaces corresponds to Werner states with different $\nu$ as indicated. In (a), the PDL of channel $B$ is fixed at $p_B = 3$ dB. In (b), the magnitudes of the two PDL elements are kept equal.

for the following analysis. Since the Bell-diagonal states have diagonal coherence matrices, the transformations given by $\boldsymbol{T}$ can consist of both reflections and reductions in length along all three axes in Stokes space.

We can now use a geometrical interpretation of Eq. (7) to find the extreme values of $\kappa$. From Eq. (7), we see that the extreme values depend on the magnitude of $||\boldsymbol{T}\hat{\gamma}_A||$ and the orientation of $\hat{\gamma}_B$ with respect to $\boldsymbol{T}\hat{\gamma}_A$, represented by the variable $\theta$. The magnitude of $||\boldsymbol{T}\hat{\gamma}_A||$ is maximized when $\hat{\gamma}_A$ is along the direction in Stokes space corresponding to the largest $|t_i|$ value in $\boldsymbol{T}$, so that $||\boldsymbol{T}\hat{\gamma}_A|| = \text{Max}[|t_i|]$. If two of the $|t_i|$ equally take the largest value, then $\hat{\gamma}_A$ can point anywhere in the plane defined by them. If all three $|t_i|$ are equal, then no orientation is preferred. The extreme values of $\kappa$, which we denote as $\kappa^E$, are therefore given by:

$$\kappa^E = \pm\text{Max}[|t_i|], \qquad (8)$$

where the $\pm$ corresponds to $\theta = 0, \pi$. As mentioned in Section II-A, Bell states satisfy the condition that all three $|t_i| = 1$; hence, it follows from from Eq. (8) that $\kappa^E_{Bell} = \pm 1$. On the other hand, Werner states satisfy the condition that all $|t_i| = \nu$, thus $\kappa^E_W = \pm\nu$. As for rank-2 Bell-diagonal states, they have a single $|t_i| = 1$ and two $|t_{j \neq i}| = C_{R2}$. In this case, the range of $\kappa$ again returns to that of a Bell state and is given
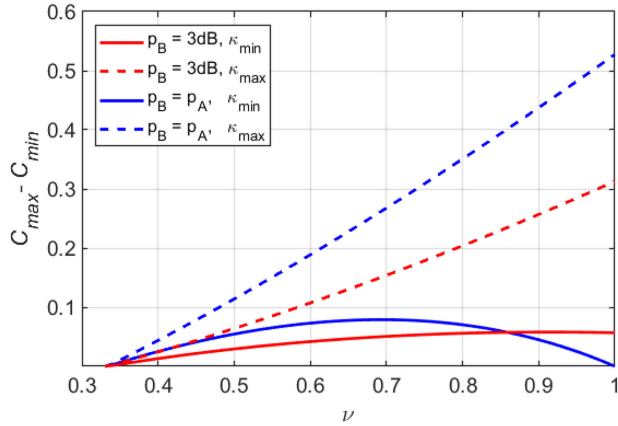
Fig. 2. Variation in concurrence of Werner states as a function of $\nu$ along lines of $\kappa = \pm\nu$ in Fig. 1. The red lines correspond to Fig. 1(a) and the blue lines to Fig. 1(b), while the solid lines are for $\kappa = -\nu$ and the dashed are for $\kappa = \nu$.

by $\kappa_{R2}^E = \pm 1$, even though the state is mixed and imperfectly entangled.

Now, we visualize how the range of $\kappa$ impacts the concurrence of entangled states. In Fig. 1, we plot Eq. (3) as a function of both PDL and $\kappa$. Colored surfaces represent different initial states, each being a Werner state with $\nu = 1, 0.68, 0.44, 0.33$. The gradual progression of colors from green to blue corresponds to decreasing $\nu$ and an increasing amount of noise. The topmost green surface is the ideal scenario of the initial state being a Bell state ($\nu = 1$). In Fig. 1(a), the PDL magnitude in channel $B$, notated in dB as $p_B = \gamma_B (20 \log_{10} e)$, is held fixed at 3 dB, while the magnitude of the PDL in channel $A$, notated in dB as $p_A$, is varied from 0 to 6 dB. Fig. 1(b) shows similar surface plots, but the magnitude of $p_A$ and $p_B$ are increasing simultaneously such that $p_A = p_B$. The $\kappa$ axes should be interpreted as parameterizing all possible orientations of the two PDL elements. The red line in Fig. 1(a) is along $\kappa = -\nu = -1$ for the $\nu = 1$ surface and physically corresponds to the case where $\boldsymbol{T}\hat{\gamma}_A$ and $\hat{\gamma}_B$ are anti-aligned. We see that the peak concurrence value occurs along this red line near $p_A = p_B = 3$ dB. Likewise, in Fig. 1(b) where $p_A = p_B$, the topmost surface corresponding to a Bell state returns to $C = 1$ for the entire $\kappa = -1$ (red) line. This nonlocal cancellation of two PDL elements is the topic of section III.

Any realistic attempt to distribute Bell states is likely to include some noise. Intuitively, the effect of PDL and its orientation should become less pronounced in the presence of depolarized noise, such as in the case of Werner states. Indeed, in both panels of Fig. 1, it is apparent that the overall effect of PDL alignment, as parameterized by $\kappa$, reduces as the Werner state becomes more mixed. This is evident by an overall flattening of the surfaces as $\nu$ decreases and by comparison of the red and purple lines along the $\kappa = -\nu$ edges of each plot. The flattening is represented more clearly in Fig. 2, where the difference between the maximum and minimum concurrences of Fig. 1(a) and (b) along the $\kappa = \pm\nu$ lines are plotted as a function of $\nu$. The dashed (solid) lines represent the $\kappa = \nu$ ($\kappa = -\nu$) lines, and the red and blue lines correspond to the system configurations of Fig. 1(a) and (b), respectively. The dashed and solid

lines can be thought of as representing the cases where the two PDL elements, one in each channel, nonlocally add together or cancel each other out, respectively. We see that the dependence of concurrence on PDL is relatively small in all cases, and that the effect gets smaller as the state becomes noisier. Interestingly, when $\nu = 1$, which corresponds to a Bell state, the solid blue line also goes to zero. This same effect can be seen in Fig. 1(a) where $p_A = p_B = 3$ dB, and is the topic of the next section. Therefore, the solid blue line shows that the concurrence of a state becomes less dependent on PDL orientations as $\nu \to 0$ and that two nonlocal PDL elements can be arranged such that they do not reduce the concurrence when $\nu \to 1$.

## III. NONLOCAL COMPENSATION OF POLARIZATION DEPENDENT LOSS

In this section, we further explore how the concurrence of a state is fully or partially restored when two PDL elements, one acting on each qubit of the entangled state, are properly aligned. We term this nonlocal PDL compensation and derive the optimal magnitude of PDL that must be inserted into one channel in order to recover the maximum amount of the concurrence lost due to PDL in another channel. We further give explicit expressions for the maximum amount of concurrence that can be recovered with this strategy and describe under what conditions the compensation is perfect.

It is well-known that, in the classical case, two partial polarizers of equal magnitude and orthogonal orientation placed in series negate each other and act as pure loss. However, it is somewhat surprising to envision two nonlocal polarizing elements, that is two elements in separate channels, acting as pure loss in a similar fashion. As we describe below the nonlocal compensation of PDL can be viewed in a manner analogous to two polarizers placed in series with the cancellation mediated by the nonlocal nature of the state itself.

### A. Optimal Polarization Dependent Loss Element for Nonlocal Compensation

Given a system configuration with a PDL of magnitude $\gamma_A$ in one channel, we determine the optimal magnitude $\gamma_B^{opt}$ of a PDL element inserted in the other channel, in order to maximize the concurrence of the final state after each photon is transmitted through its respective channel. To achieve this, we minimize the denominator of Eq. (3) while assuming a fixed $\gamma_A$. Although minimization can be performed simultaneously over both $\kappa$ and $\gamma_B$, it is not necessary. For all $\gamma_{A,B} \geq 0$, $\cosh(\gamma_A)\cosh(\gamma_B) > \sinh(\gamma_A)\sinh(\gamma_B) \geq 0$. Therefore, since $|\kappa| \leq 1$, the expression $\cosh(\gamma_A)\cosh(\gamma_B) + \kappa \sinh(\gamma_A)\sinh(\gamma_B)$ is minimized when $\kappa$ is negative and takes an extreme value ($\kappa^E$). Therefore, the denominator of Eq. (3) only needs to be minimized over $\gamma_B$, assuming a fixed $\gamma_A$ and the minimum possible $\kappa = -|\kappa^E|$. To facilitate the minimization, we define the denominator as a single variable function $f(\gamma_B) = \cosh(\gamma_A)\cosh(\gamma_B) - |\kappa^E|\sinh(\gamma_A)\sinh(\gamma_B)$, and solve $\frac{df(\gamma_B)}{d\gamma_B} = 0$, resulting in:

$$\gamma_B^{opt} = \tanh^{-1}\left(|\kappa^E|\tanh(\gamma_A)\right). \tag{9}$$
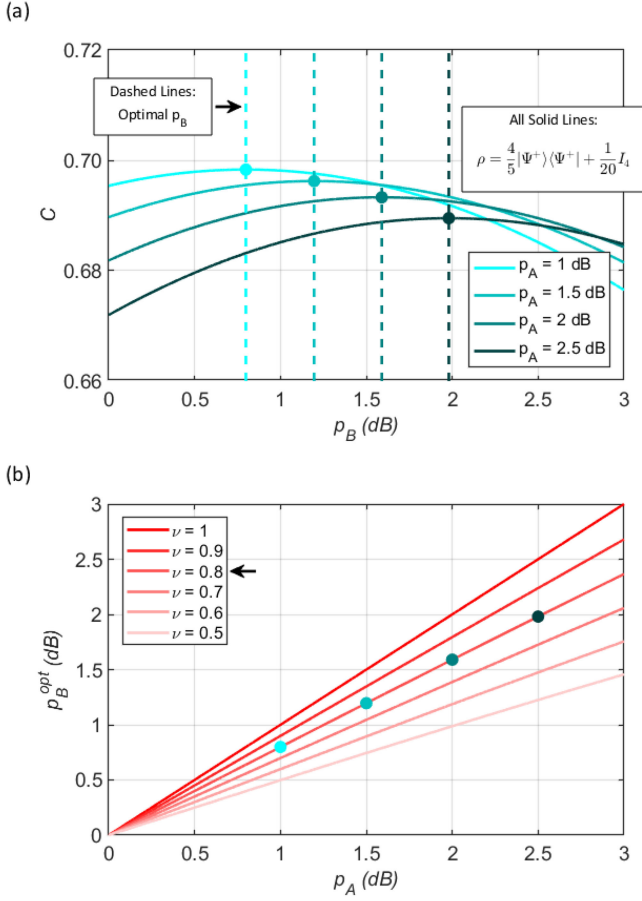
(a)



(b)



Fig. 3. (a) Concurrence as a function of the magnitude of the compensating PDL element $p_B$ for a specific Werner state. Colors denote a varying amount of fixed PDL in channel A, $p_A$. The vertical dashed lines indicate the optimal $p_B$ value corresponding to maximum concurrence. (b) Optimal compensating value $p_B^{opt}$ in channel B vs the magnitude of PDL $p_A$ in channel A for several Werner states with an increasing amount of noise. Symbols in both plots correspond to the optimal $p_B$ values for the $\nu = \frac{4}{5}$ case.

Therefore, optimal nonlocal compensation occurs when the PDL elements are oriented such that $\kappa = -|\kappa_E|$ and the compensating element is tuned to the value $\gamma_B^{opt}$ given in Eq. (9). An inability to obtain either of these requirements results in a state with concurrence less than the optimal case; however, the dependence of concurrence on each of these parameters is slowly varying, as seen in Figs. 1 and 2.

To demonstrate how the optimal magnitude depends on the input state and how this affects the concurrence of the final state, we return to the three example cases from before: Bell states, Werner states, and rank-2 Bell-diagonal states. Using the $\kappa_E$ values found in Section II-B and assuming a fixed PDL of magnitude $\gamma_A$ in one channel, we find $\gamma_B^{opt} = \gamma_A$ for Bell states and rank-2 Bell-diagonal states, which concurs with the results found in [28], [29].

Alternatively, for Werner states, we find that the magnitude of the optimal compensating PDL element is less than that of the applied PDL element, and is given by $\gamma_W^{opt} = \tanh^{-1}(\nu \tanh(\gamma_A))$. This is illustrated in Figs. 3(a) and (b). In Fig. 3(a), we plot the concurrence of the same Werner state

with $\nu = \frac{4}{5}$ for four different cases of fixed PDL magnitude in channel A denoted by shades of blue ($p_A = 1, 1.5, 2, 2.5$ dB), each as a function of the magnitude of another PDL element in channel B. The optimal $p_B$ for each fixed $p_A$ are denoted by the vertical dashed lines and correspond to the peak concurrences. The values of these peak concurrences are derived in the next section. The optimal compensating value $p_B^{opt}$ for the set of applied $p_A$ values considered in Fig. 3(a) ranges from about 0.8 dB to 2 dB and is always less than $p_A$.

In Fig. 3(b), we plot the magnitude (in dB) of the optimal compensating element $p_B^{opt}$, as derived from Eq. (9), as a function of the applied PDL element $p_A$. Lines of different shades represent a family of Werner states with a gradually increasing amount of noise. The line of $\nu = \frac{4}{5}$ corresponds to the Werner states in Fig. 3(a). To better illustrate the connection between the two plots, we note that the circles in Fig. 3(a) denote four triplets of values for $p_A$, $p_B^{opt}$, and $C$. We use the same symbols and colors to indicate corresponding pairs of $p_A$ and $p_B^{opt}$ in Fig. 3(b). As an explicit example, we consider $p_A = 2$ dB for the Werner state with $\nu = \frac{4}{5}$, as used in Fig. 3(a). For this point, we see from Figs. 3(a) and (b) that the maximum concurrence after nonlocal compensation occurs when $p_B = 1.59$ dB. From this figure, it is clear that the magnitude of the optimal compensating element decreases as the Werner state becomes more mixed.

### B. Maximum Possible Concurrence After Nonlocal Compensation

Using the optimal compensating elements derived in the previous section, we calculate the concurrence of the final state after nonlocal compensation using Eq. (3). For Bell states, the final concurrence after optimal nonlocal compensation is again given by $C_{Bell}^{opt} = 1$. Therefore, a Bell state which is degraded by PDL in one channel can be brought back to a fully entangled state with the insertion of an equivalent amount of properly aligned PDL in the other channel. For the case of Werner states, we find that:

$$C_W^{opt} = \frac{3\nu - 1}{2 \cosh(\gamma_A)\sqrt{1 - \nu^2 \tanh^2(\gamma_A)}}, \quad (10)$$

for $\nu > 1/3$, meaning that the initial state is entangled. The peak points of Fig. 3(a) correspond to the value of Eq. (10) for each scenario. Finally, we find the surprising result that a rank-2 Bell-diagonal state with initial concurrence $C_{R2}$ can be brought back to this value via optimal compensation, i.e. $C_{R2}^{opt} = C_{R2}$. Therefore, it is still possible to perform perfect nonlocal compensation, despite the fact that the rank-2 state is imperfectly entangled and mixed. This is a practically significant result because Bell states undergoing common decoherence mechanisms in optical fibers become rank-2 Bell-diagonal states [23].

More generally, the concurrence of a Bell-diagonal state $\boldsymbol{\rho}_{BD}$ after optimal nonlocal compensation is given by:

$$C_{BD}^{opt} = \frac{\cosh(\gamma_B^{opt})}{\cosh(\gamma_A)} C(\boldsymbol{\rho}_{BD}), \quad (11)$$

where the ratio $\frac{\cosh(\gamma_B^{opt})}{\cosh(\gamma_A)} \leq 1$.
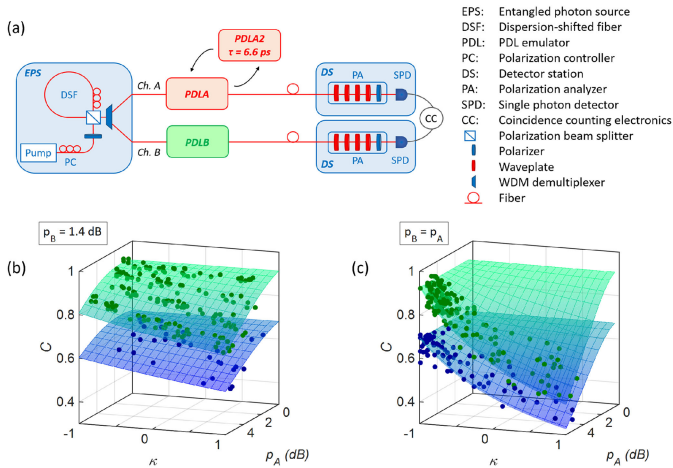
Fig. 4.    (a) Experiment schematics. (b, c) Concurrence as a function of $\kappa$ and applied PDL in channel A, $p_A$. Symbols show experimental data, and surface plots show theory. Blue denotes the presence and green denotes the absence of an additional differential group delay of $\tau = 6.6$ ps in channel A. The PDL of channel B is constant, $p_B = 1.4$ dB, in (b) and equal to that of channel A, $p_A = p_B$, in (c).

## IV. EXPERIMENT

A diagram of our experiment is shown in Fig. 4(a). Our fiber-based testbed includes an entangled photon source (EPS) [30], two detector stations (DS), and PDL emulating/compensating modules (PDLA, PDLA2, PDLB) that are inserted into channels A and B as needed. All of the modules are fully tunable in Stokes orientation and PDL magnitude (0 dB − 7 dB). In addition to PDL, one of the modules (PDLA2) also introduces a differential group delay of $\tau = 6.6$ ps.

Signal and idler photons are created by the EPS via four-wave mixing by pumping a dispersion shifted fiber (DSF) with a 50 MHz pulsed fiber laser operating at 193.1 THz [31], [32]. The DSF is arranged in the Sagnac configuration using a polarization beam splitter (PBS), and a WDM demux placed at the output of the Sagnac loop filters out the pump and separates photons spectrally into 100 GHz-spaced ITU outputs [32]. The average number of generated photon pairs per pulse is tunable within a range of $0.001 - 0.1$ [33], [34]. Detector stations consisting of a polarization analyzer (PA) and an InGaAs single photon detector (SPD) detect photons at the output of channels A and B. The detectors have a detection efficiency of $\eta \sim 20\%$ and a dark count probability of $\sim 4 \times 10^{-5}$ per gate. Automated FPGA-based controller software performs full polarization state tomography [35], [36] in order to determine the density matrix of the state generated by the EPS.

To characterize our source, we connect both detector stations directly back-to-back (B2B) to it, perform state tomography, and then calculate the concurrence of the resulting density matrix. The B2B concurrence is $0.925 \pm 0.008$. Noise photons generated by Raman scattering in the DSF and pump leakage into the entangled photon band are primarily responsible for the decrease of the concurrence from unity [32], [37]. In order to consider the practical case of a Bell state partially degraded by PMD, we utilize a special PDL emulator (PDLA2) between

the EPS and detector station in channel A. This emulator has a fixed differential group delay of $\tau = 6.6$ ps in addition to variable PDL. When applying PMD to channel A with PDLA2 (but setting the PDL magnitude of PDLA2 to zero), the measured state is a rank-2 Bell-diagonal state with a reduced concurrence of $0.690 \pm 0.010$.

In order to verify the dependence of entanglement quality on applied PDL derived in Section II, we start with an experimental setup that has a variable PDL module inserted into channel A, shown as the red PDLA box in Fig. 4(a), and a fixed PDL in channel B given by $p_B = 1.4$ dB. We set the PDL of channel A to five different PDL magnitudes of 1.25, 2.55, 3.7, 5.1, and 6.3 dB using PDLA. At each PDL value, the orientation of the PDL of channel A in Stokes space is varied such that the the vector $\vec{\gamma}^A$ covers the Poincare sphere. The state's concurrence $C$ and the variable $\kappa$ are calculated for each setting from density matrices obtained by performing state tomography. The resulting data are plotted as green points in Fig. 4(b) along with a surface plot that is similar to those presented in Fig. 1. The green surface is calculated from Eq. (3) with an initial concurrence of $C(\boldsymbol{\rho}_0) = 0.925$, which is the experimentally-attained value with $p_A = p_B = 0$. The chosen range of $\kappa$ corresponds to the ideal case of a Bell state: $-1 \leq \kappa \leq 1$.

Next, we replace the PDLA module with the module PDLA2 that has a fixed amount of first order PMD in addition to the variable PDL. Following the same protocol as described above, we obtain the data presented with the blue points in Fig. 4(b). Here, the blue surface is also calculated from Eq. (3) and covers the same range of $-1 \leq \kappa \leq 1$, but it has an initial concurrence of $C(\boldsymbol{\rho}_0) = 0.690$. The latter is the experimentally-attained value of the concurrence for our rank-2 Bell-diagonal state for $p_A = p_B = 0$. Here, PMD is addressed by considering our state as a rank-2 Bell-diagonal state resulting from PMD applied to one qubit of a Bell state. The applied PDL is then considered after the application of PMD. A more rigorous treatment of the interaction of PMD and PDL is planned for a future project. For each of the two specific cases of the general Bell-diagonal state, that is for a nearly perfect Bell state (green) and for a rank-2 Bell-diagonal state (blue), our experimental data is in excellent agreement with a calculation based on Eq. (3). Thus, the data clearly support our theoretical results.

Now we modify our setup to utilize two variable PDL emulators in order to demonstrate nonlocal PDL compensation, as described in Section III. We revert back to the original setup with no PMD; that is, PDLA and PDLB are inserted in channels A and B respectively, but now we operate each emulator in a different manner. First, we set the magnitude of the PDL of channel A to one of 15 different values ranging from 4.12–6.38 dB, and we fix the orientation of the PDL element for each magnitude. Then, we set the magnitude of the emulator PDLB to be equal to the PDL of channel A. Next, we adjust the orientation of PDLB to several different settings for each value of the PDL of channel A using a polarization controller contained within the module PDLB, and we perform tomography for each setting. Once again, we calculate the concurrence $C$ and the variable $\kappa$ from the resulting density matrices, and we plot these results with green points in Fig. 4(c). For $\kappa = -1$, there is no decrease
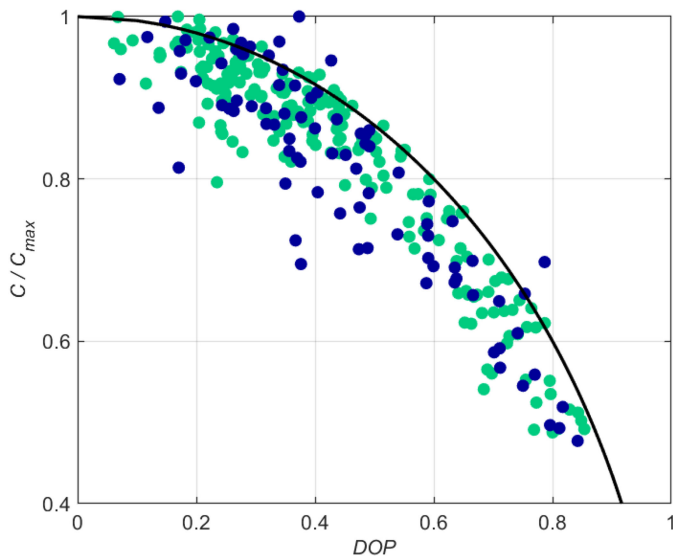
Fig. 5. Normalized concurrence $C/C_{\max}$ as a function of the DOP of photon A for the data of Fig. 4(c). The same color scheme codes the absence (green) or presence (blue) of PMD in channel A. The black line denotes the theory.

in concurrence for all magnitudes of $p_A = p_B$, thus demonstrating the nonlocal compensation described in Section III.

As our final setup modification, we once again replace the PDLA module with the module PDLA2 which introduces PMD. To investigate nonlocal PDL compensation for a rank-2 Bell-diagonal state, we follow the same procedure described above for 12 different settings of $p_A = p_B$ ranging from 4.60–6.01 dB and plot the results with the blue points in Fig. 4(c). Our experiment proves that the initial concurrence of $C_{R2} = 0.690$ at $p_A = p_B = 0$ is again largely restored for all experimentally available PDL magnitudes, as long as $p_A = p_B$ and $\kappa = -1$.

Finally, we consider an alternative means to determine the optimal settings of PDLA and PDLB for nonlocal PDL compensation using the reduced density matrices which describe individual photons in the two-qubit entangled state. So far, we have only considered maximizing the calculated concurrence, a two-photon metric, in order to find the optimum orientation of PDLB. Now, we examine the degree of polarization (DOP) of an individual photon (calculated from the reduced density matrix) of the entangled pair. The black line in Fig. 5 depicts the theoretical normalized concurrence as a function of the DOP of photon A. Now, consider all compensation data points shown in Fig. 4(b). The green points in Fig. 5 show the normalized concurrence vs the DOP of photon A for each of these points taken without PMD. Likewise, the blue points in Fig. 5 show the normalized concurrence vs. DOP of photon A for the data set in which compensation was performed with PMD applied to channel A via the emulator PDLA2. Here, the concurrence values are normalized to the concurrence when $p_A = p_B = 0$, such that the maximum value is given by $C/C_{\max} = 1$. Fig. 5 shows that as the DOP of photon A is decreased, the optimum orientation of PDLB is approached, and the concurrence increases, thus compensating for the effects of PDLA (or PDLA2). The blue data of Fig. 5 are an explicit demonstration of an earlier

theory proposed in [17], [19], [20] that a two-photon *mixed* state achieves its maximum entanglement under local filtering operations when the reduced density matrices become depolarized. Furthermore, the data suggest that the depolarization of an individual photon, found by tracing away one qubit of a measured two-qubit density matrix, could serve as a form of feedback for nonlocal PDL compensation.

## V. CONCLUSION

We consider the deleterious effects of PDL in fiber-optic networks on propagating two-photon quantum states. Our rigorous theoretical treatment encompasses a wide class of states known as Bell-diagonal states. For these states, we establish the dependence of the principal entanglement metric, the state concurrence, on PDL of arbitrary orientation and magnitude. We then analyze the effects of PDL on particular subclasses of states that could arise either from added depolarized noise or from decoherence during fiber propagation. Specifically, we examine the behavior of Werner states, rank-2 Bell diagonal states, and ideal Bell states. We further verify our theory experimentally for the latter two cases. Finally, we examine how the PDL acting on each photon of a two-photon quantum state interacts with each other and how this interaction could lead to loss and recovery of the entanglement of the two-photon state.

## REFERENCES

[1] R. Van Meter, *Quantum Networking*. New York, NY, USA: Wiley, 2014. [Online]. Available: https://books.google.com/books?id=khmNAwAAQBAJ
[2] B. T. Kirby, S. Santra, V. S. Malinovsky, and M. Brodsky, "Entanglement swapping of two arbitrarily degraded entangled states," *Phys. Rev. A*, vol. 94, no. 1, 2016, Art. no. 012336.
[3] J. N. Damask, *Polarization Optics in Telecommunications*, vol. 101. Berlin, Germany: Springer Science + Business Media, 2004.
[4] M. Brodsky, N. J. Frigo, M. Boroditsky, and M. Tur, "Polarization Mode Dispersion of installed fibers," *J. Lightw. Technol.*, vol. 24, no. 12, pp. 4584–4599, Dec. 2006.
[5] M. Brodsky, N. J. Frigo, and M. Tur, "Polarization mode dispersion," in *Optical Fiber Telecommunications V A*, I. P. Kaminow, T. Li, and A. E. Willner, Eds., 5th ed. Burlington, NJ, USA: Academic, 2008, ch. 17, pp. 605–669.
[6] N. Gisin, "Statistics of polarization dependent losses," *Opt. Commun.*, vol. 114, no. 5/6, pp. 399–405, 1995.
[7] A. Mecozzi and M. Shtaif, "The statistics of polarization-dependent loss in optical communication systems," *IEEE Photon. Technol. Lett.*, vol. 14, no. 3, pp. 313–315, Mar. 2002.
[8] A. Galtarossa and L. Palmieri, "The exact statistics of polarization-dependent loss in fiber-optic links," *IEEE Photon. Technol. Lett.*, vol. 15, no. 1, pp. 57–59, Jan. 2003.
[9] C. Vinegoni, M. Karlsson, M. Petersson, and H. Sunnerud, "The statistics of polarization-dependent loss in a recirculating loop," *J. Lightw. Technol.*, vol. 22, no. 4, pp. 968–976, Apr. 2004.
[10] O. Liboiron-Ladouceur, K. Bergman, M. Boroditsky, and M. Brodsky, "Polarization-dependent gain in SOA-based optical multistage interconnection networks," *J. Lightw. Technol.*, vol. 24, no. 11, pp. 3959–3967, Nov. 2006.
[11] M. Shtaif and O. Rosenberg, "Polarization-dependent loss as a waveform-distorting mechanism and its effect on fiber-optic systems," *J. Lightw. Technol.*, vol. 23, no. 2, pp. 923–930, Feb. 2005.

[12] M. Shtaif, "Performance degradation in coherent polarization multiplexed systems as a result of polarization dependent loss," *Opt. Express*, vol. 16, no. 18, pp. 13918–13932, 2008.

[13] M. Medic and P. Kumar, "Effects of polarization-dependent loss and fiber birefringence on photon-pair entanglement in fiber-optic channels," in *Proc. Photon. Appl. Syst. Technol. Conf.*, 2007, Paper JTuA16.

[14] N. Gisin, "Hidden quantum nonlocality revealed by local filters," *Phys. Lett. A*, vol. 210, no. 3, pp. 151–156, 1996.

[15] N. Linden, S. Massar, and S. Popescu, "Purifying noisy entanglement requires collective measurements," *Phys. Rev. Lett.*, vol. 81, no. 15, pp. 3279–3282, 1998.

[16] A. Kent, "Entangled mixed states and local purification," *Phys. Rev. Lett.*, vol. 81, no. 14, pp. 2839–2841, 1998.

[17] A. Kent, N. Linden, and S. Massar, "Optimal entanglement enhancement for mixed states," *Phys. Rev. Lett.*, vol. 83, no. 13, pp. 2656–2659, 1999.

[18] F. Verstraete, J. Dehaene, and B. DeMoor, "Local filtering operations on two qubits," *Phys. Rev. A*, vol. 64, no. 1, 2001, Art. no. 010101.

[19] R. Thew and W. Munro, "Entanglement manipulation and concentration," *Phys. Rev. A*, vol. 63, no. 3, 2001, Art. no. 030302.

[20] R. Thew and W. Munro, "Mixed state entanglement: Manipulating polarization-entangled photons," *Phys. Rev. A*, vol. 64, no. 2, 2001, Art. no. 022320.

[21] P. G. Kwiat, S. Barraza-Lopez, A. Stefanov, and N. Gisin, "Experimental entanglement distillation and 'hidden' non-locality," *Nature*, vol. 409, no. 6823, pp. 1014–1017, 2001.

[22] C. Antonelli, M. Shtaif, and M. Brodsky, "Sudden death of entanglement induced by polarization mode dispersion," *Phys. Rev. Lett.*, vol. 106, Feb. 2011, Art. no. 080404.

[23] M. Brodsky, E. C. George, C. Antonelli, and M. Shtaif, "Loss of polarization entanglement in a fiber-optic system with polarization mode dispersion in one optical path," *Opt. Lett.*, vol. 36, no. 1, pp. 43–45, 2011.

[24] M. Shtaif, C. Antonelli, and M. Brodsky, "Nonlocal compensation of polarization mode dispersion in the transmission of polarization entangled photons," *Opt. Express*, vol. 19, no. 3, pp. 1728–1733, 2011.

[25] R. Horodecki and M. Horodecki, "Information-theoretic aspects of inseparability of mixed states," *Phys. Rev. A*, vol. 54, no. 3, pp. 1838–1843, 1996.

[26] W. K. Wootters, "Entanglement of formation of an arbitrary state of two qubits," *Phys. Rev. Lett.*, vol. 80, no. 10, pp. 2245–2248, 1998.

[27] Q. Quan, H. Zhu, S.-Y. Liu, S.-M. Fei, H. Fan, and W.-L. Yang, "Steering bell-diagonal states," *Sci. Rep.*, vol. 6, 2018, Art. no. 22025.

[28] D. E. Jones, B. T. Kirby, and M. Brodsky, "Polarization dependent loss in optical fibers-does it help or ruin photon entanglement distribution?" in *Proc. Opt. Fiber Commun. Conf.* 2018, Paper Th4B–1.

[29] D. E. Jones, B. T. Kirby, and M. Brodsky, "Tuning quantum channels to maximize polarization entanglement for telecom photon pairs," *npj Quantum Inf.*, vol. 4, no. 58, Nov. 2018.

[30] NuCrypt, "Quantum optical instrumentation." 2018. [Online]. Available: http://nucrypt.net/quantum-optical-instrumentation.html

[31] M. Fiorentino, P. L. Voss, J. E. Sharping, and P. Kumar, "All-fiber photon-pair source for quantum communications," *IEEE Photon. Technol. Lett.*, vol. 14, no. 7, pp. 983–985, Jul. 2002.

[32] S. X. Wang and G. S. Kanter, "Robust multiwavelength all-fiber source of polarization-entangled photons with built-in analyzer alignment signal," *IEEE J. Sel. Top. Quantum Electron.*, vol. 15, no. 6, pp. 1733–1740, Nov./Dec. 2009.

[33] D. E. Jones, B. T. Kirby, and M. Brodsky, "Joint characterization of two single photon detectors with a fiber-based source of entangled photon pairs," in *Proc. Frontiers Opt.* 2017, Paper JW4A–37.

[34] D. E. Jones, B. T. Kirby, and M. Brodsky, "In-situ calibration of fiber-optics entangled photon distribution system," in *Proc. IEEE Photon. Soc. Summer Topical Meeting Ser.*, 2017, pp. 123–124.

[35] A. G. White, D. F. James, P. H. Eberhard, and P. G. Kwiat, "Nonmaximally entangled states: Production, characterization, and utilization," *Phys. Rev. Lett.*, vol. 83, no. 16, pp. 3103–3107, 1999.

[36] D. F. V. James, P. G. Kwiat, W. J. Munro, and A. G. White, "Measurement of qubits," *Phys. Rev. A*, vol. 64, Oct. 2001, Art. no. 052312.

[37] X. Li, P. L. Voss, J. Chen, K. F. Lee, and P. Kumar, "Measurement of co-and cross-polarized raman spectra in silica fiber for small detunings," *Opt. Express*, vol. 13, no. 6, pp. 2236–2244, 2005.

**Brian T. Kirby** received the B.S. degree in physics from Towson University, Towson, MD, USA, in 2010, and the M.S. and Ph.D. degrees in physics from the University of Maryland—Baltimore County, Baltimore, MD, USA, in 2012 and 2015, respectively. He joined the U.S. Army Research Laboratory as a Postdoctoral Researcher in 2015 and became a Staff Scientist in 2016. His main research interests are in quantum networking and optical quantum information processing.

**Daniel E. Jones** received the B.A. degree in physics from McDaniel College, Westminster, MD, USA, in 2010, and the M.S. and Ph.D. degrees in physics from the University of Maryland—Baltimore County, Baltimore, MD, USA, in 2012 and 2016, respectively. He joined the U.S. Army Research Laboratory as a Postdoctoral Researcher in 2016 and became a Staff Scientist in 2018. His main research interests are in quantum networking, quantum and nonlinear optics, and the physics of fiber propagation.

Dr. Jones is a Member of the Optical Society of America.

**Michael Brodsky** joined the U.S. Army Research Laboratory in 2014 to lead research in quantum networks. Michaels current prime research interests are quantum communications and networks, photon entanglement and entanglement decoherence, and quantum information processing. Prior to that, he was a member of technical staff at AT&T Labs, where his contributions to fiber optic communications were focused on optical transmission systems and the physics of fiber propagation, most notably through his work on polarization effects in fiber-optic networks. Dr. Brodsky has authored or co-authored over 100 journal and conference papers, a book chapter and holds about 35 granted U.S. patents. He served as a topical editor for Optics Letters and has been active on numerous program committees for IEEE Photonics Society and OSA conferences.

Dr. Brodsky is a Fellow of OSA and holds a PhD in Physics from MIT.